LAWRENCE
LIVERMORE
NATIONAL
LABORATORY

UCRL-JRNL-204488

Dosimetry for quantitative analysis of low dose ionizing radiation effects on humans in radiation therapy patients

J. Lehmann, R. L. Stern, T. P. Daly, C. W. Schwieter, G. E. Jones, M. L. Arnold, C. L. Hartmann-Siantar, Z. Goldberg

June 4, 2004

Radiation Research Journal

This document was prepared as an account of work sponsored by an agency of the United States Government. Neither the United States Government nor the University of California nor any of their employees, makes any warranty, express or implied, or assumes any legal liability or responsibility for the accuracy, completeness, or usefulness of any information, apparatus, product, or process disclosed, or represents that its use would not infringe privately owned rights. Reference herein to any specific commercial product, process, or service by trade name, trademark, manufacturer, or otherwise, does not necessarily constitute or imply its endorsement, recommendation, or favoring by the United States Government or the University of California. The views and opinions of authors expressed herein do not necessarily state or reflect those of the United States Government or the University of California, and shall not be used for advertising or product endorsement purposes.

Dosimetry for quantitative analysis of low dose ionizing radiation effects on humans in radiation therapy patients

Joerg Lehmann [a,b 1], Robin L. Stern [b], Thomas P. Daly [a], Chad W. Schwietert [b], Gregory E. Jones [c], Michelle L. Arnold [a], Christine L. Hartmann Siantar [a,b], Zelanna Goldberg [b]

[a] Glenn T. Seaborg Institute, University of California – Lawrence Livermore National Laboratory, Livermore, CA, USA

[b] Department of Radiation Oncology, University of California Davis Cancer Center, Sacramento, CA, USA

[c] Hazards Control and Safety Program, University of California – Lawrence Livermore National Laboratory, Livermore, CA, USA

8 figures and 0 tables are submitted

Suggested running title: Dosimetry for LDIR studies in radiation therapy patients

Corresponding Author: Joerg Lehmann, Ph.D.
UC - Lawrence Livermore National Laboratory
7000 East Ave,
L-231
Livermore, CA 94550

Phone: (925) 422-2741
Fax: (925) 423-9719
Email: jlehmann@llnl.gov

Lehmann, J., Stern, R. L., Daly, T. P., Schwietert, C. W., Jones, G. E., Arnold, M. L., Hartmann Siantar, C. L., Goldberg, Z., Dosimetry for quantitative analysis of low dose ionizing radiation effects on humans in radiation therapy patients. *Radiat. Res.*

We have successfully developed a practical approach to predicting the location of skin surface dose at potential biopsy sites that receive 1 cGy and 10 cGy, respectively, in support of in vivo biologic dosimetry in humans. This represents a significant technical challenge as the sites lie on the patient surface outside the radiation fields. The PEREGRINE Monte Carlo simulation system was used to model radiation dose delivery and TLDs were used for validation on a phantom and confirmation during patient treatment. In the developmental studies the Monte Carlo simulations consistently underestimated the dose at the biopsy site by approximately 15% for a realistic treatment configuration, most likely due to lack of detail in the simulation of the linear accelerator outside the main beam line. Using a single, thickness-independent correction factor for the clinical calculations, the average of 36 measurements for the predicted 1 cGy point was 0.985 cGy (standard deviation: 0.110 cGy) despite patient breathing motion and other real world challenges. Since the 10 cGy point is situated in the region of high dose gradient at the edge of the field, patient motion had a greater effect and the six measured points averaged 5.90 cGy (standard deviation: 1.01 cGy), a difference that is equivalent to approximately a 6 mm shift on the patient's surface.

INTRODUCTION

The long term effects of low dose ionizing radiation (LDIR) on the human body have been studied based on data from the survivors of radiological accidents and the atomic bomb detonations in Hiroshima and Nagasaki in August 1945. A linear relationship between increased cancer risk and single radiation dose has been established for the dose range from 0.5 Sv to approximately 2.5 Sv. Below 0.5 Sv, theories regarding relative biologic effectiveness vary widely from bystander effect, predicting a proportionally higher risk from low doses, to hormesis, postulating a positive effect from LDIR. Knowledge of the potential biologic effects of LDIR is highly desirable as it impacts risk assessment for a range of industrial applications and clinical procedures which use ionizing radiation. Current public policy in the United States is based on the "linear no-threshold model" which assumes that the effects of LDIR can be estimated by linear extrapolation backwards from effects observed for high doses. A conclusion of this model is the belief that there is no safe dose as even very low doses of ionizing radiation produce some (assumed negative) biological effect.

There is ample evidence from in vitro cell culture models that doses as low as 1 cGy result in biologic activity (*1*). However, the cells used in such studies lack the complexity of 3-dimensional tissue. In addition, cell lines have often been immortalized or transformed and live on artificial substrates. To draw conclusions with respect to the effect of LDIR on the human body it is therefore necessary to obtain translational data in humans. It is not possible to irradiate volunteers prospectively for the purpose of such studies; however, humans are irradiated daily for the treatment of their cancers, providing a population where prospective data can be obtained. In fact, radiotherapy patient volunteers offer a wide range of dose points if the physics and dosimetric support for site

identification is sufficiently robust. As the specimens would be obtained from cancer patients receiving therapeutic radiation, the dose delivered cannot be altered for ease of scientific protocols. Consequently, LDIR exposure is generally received outside the radiation treatment area, making the dosimetry a significant challenge.

To assess the biological effects of low dose radiation on humans, skin may be sampled outside the primary radiation fields in areas that still receive quantifiable doses (*2*). Skin is a good model tissue as it is easily accessible for biopsy in the clinic. Most solid tumors arise from epithelial tissue, which is modeled in the skin. For the biologic studies to provide meaningful data, the accuracy of determining the radiation dose to the tissue is paramount especially given the expectation of biologic variability. To increase the confidence that the description of the biological effect is a true finding it is important to have high confidence in the accuracy of the precision of the low dose exposure.

Clinical dosimetric treatment planning is focused on the accuracy of dose within the primary radiation fields, whose edges are defined at the 50% isodose line by convention (*3*). For this study, calculation of the dose outside the primary radiation field, in the so-called peripheral region, is of foremost interest. The sources of peripheral dose are (a) leakage from the treatment unit, (b) scatter from the primary collimator and the flattening filter, (c) scatter from the secondary collimators and from beam modifiers such as wedges, blocks, and the multileaf collimators (MLC), and (d) internal scatter originating in the patient.

Standard treatment planning systems are based on numerical approximation algorithms to calculate the dose within the radiation field fast and reasonably accurately for the purposes of the treatment. They do not attempt to address the dose outside the field with as much accuracy. Analytical algorithms connected with previous work on

peripheral dose were designed for radiation protection and therefore did not aim for the accuracy currently being sought (*4-22*).

In these studies we have used Monte Carlo simulations to obtain the accuracy needed for meaningful radiobiologic assessment of LDIR effects in the 1-10 cGy range. Given the location and the dose (as low as 0.5% of the prescribed dose), the expected uncertainties were higher than the uncertainties accepted within a treatment field. The goal of these studies was to predict sample points on the volunteer patient's skin surface with a dosimetric uncertainty of 15% or better.

MATERIALS AND METHODS

1. Monte Carlo System

The PEREGRINE Monte Carlo system was chosen for the study (*23*). A research version of the system was commissioned to simulate the 18 MV beam of a Varian Clinac 2100 (Varian Medical Systems, Palo Alto, CA) at the UC Davis Cancer Center. Simulation parameters and machine specific calibration methods are described in reference (*23*).

2. Selection of beam shaping mechanism

Since the points of dose interest were located beyond the field boundaries, the method of field shaping needed to be addressed. While the jaws function as the major field shaping tool, there are two options for the secondary field shaping tools at our clinic: Cerrobend® blocks and Multileaf Collimators (MLC). Blocks shape the radiation field within the rectilinear region described by the jaws. They normally extend only slightly beyond this region, under the jaws. Since the dose points of interest are located under the jaw, the outside edge of a block would have to be modeled precisely in the Monte Carlo code. This is not practical because the blocks are made individually and the position and shape of their outer edge vary slightly from case to case. Another option would be to extend the

block to cover the area of interest completely, thus eliminating the influence of its outer edge. This proved not to be viable as well, since block weight became excessive and the production tolerances were prohibitively high. MLCs are very reproducible, but Varian's MLC has gear mechanisms and movable banks in the direction of leaf travel which are very difficult to model. Therefore we chose to locate the biopsy points outside the field perpendicular to the MLC travel direction. For the treatment site in the initial study this was possible without impacting the overall patient treatment strategy.

While the positions of the leaves within the field were dictated by the treatment plan, there are multiple options for those leaves not involved in field shaping. Of special interest were those leaves under the Y2 jaw[1], since the dose points of interest are under that jaw. Due to the construction of the MLC, those leaves could not be completely retracted (i.e. be in the "parked" position). The standard position for them usually defaults to be "closed", abutting at the center line of the field axis (see Figure 1a). This position was not desirable for our measurements because we wanted to position the biopsy points along this axis to simplyfy their identification on the patient. Dose accuracy to the degree necessary for studying LDIR at the doses discussed here is difficult to achieve in the simulation under abutting rounded edge MLC leaves, due to the positioning uncertainty of the leaves. Two more favorable scenarios are shown in Figures 1b and c. Here the MLC leaves under the Y2 jaw are either open, that is all leaves are set to 6 cm from central axis (Figure 1b), or they are closed but abut away from the field axis, i.e. the MLC pairs are set to "–7, 7" (Figure 1c). Since we did not find any dosimetric advantage in the open case, and it gives slightly more radiation to the patient, we used the MLC closed position (Figure 1c) for our studies.

3. Beam direction and biopsy site location

Within a solid tissue equivalent material, the radiation dose inside the field deposited from a megavoltage photon beam - starting at the material surface - rises with depth and then reaches a plateau followed by a gradual fall off. The rise is caused by the establishment of charged particle equilibrium and the fall-off by attenuation and scattering of the primary beam. The initial approach for the biopsy site selection was to use tissue equivalent bolus material on an entry beam to move the skin surface (biopsy site) to a location of charged particle equilibrium and dose plateau. Verifiication measurements with a Farmer chamber in a plastic slab phantom revealed that outside the field, where the dose points for this study are located, such a plateau area does not exist. In fact, we found a moderately steep dose gradient near the entrance surface, which would have led to a higher uncertainty in the dose. Monte Carlo simulations and measurements, however, revealed a more favorable dose profile at the location where the beam exits the solid material. We therefore used the beam exit as the site for the biopsies (i.e., a posterior beam for biopsy on the patient's anterior skin). We also used simulations to investigate the effect on the dose of establishing electron equilibrium at the exit surface by adding increasing thicknesses of bolus material. We found that after 2.5 cm of tissue equivalent material no more change in dose was observed at the material (skin) surface. Thus, a 3 cm thick bolus material over the biopsy site was chosen for patient studies.

4. Confirmatory Measurements with TLDs

For the purposes of biopsy site selection in patients, Monte Carlo simulations were evaluated for their ability to accurately predict the low doses received by the skin outside the treatment field. Therefore, a detector was needed which was sensitive down to 1 cGy,

while maintaining reasonable accuracy at such low doses. The detector also needed to be small in size to avoid dose averaging. The steep dose gradient outside the field made dose averaging a significant potential complication. Ideally, the detector should be the size of the biopsy core, which is three millimeters in diameter. Thermoluminescent dosimeters (TLD) type EXT-RAD 740 (Harshaw – Thermo RMP, 6801 Cochran Road, Solon, OH 44139, USA) were used for this study. This model uses a single 7LiF:Mg,Ti chip (3x3 mm^2, TLD-700 material) permanently mounted on a bar-coded substrate. The chip thickness is 40 mg/cm^2, which corresponds to approximately 0.1 mm. The TLD chip-strate is loaded into a sealed pouch with a 0.008-inch thick window over the active portion of the TLD. Since the window is very thin the position of the chip-strate can be easily and accurately identified through it. The TLDs were read using a Harshaw model 6600 automatic TLD reader. We calibrated the TLDs using an ion chamber with known energy dependence (Farmer chamber) through measurements in a water-equivalent slab phantom. The TLDs were used for both experimental verification of our calculation methods and to verify the dose given to the patient at the biopsy site(s).

5. Validation of accuracy of Monte Carlo system

A newly designed anthropomorphic phantom (*24*) was used to investigate the accuracy of the PEREGRINE Monte Carlo system in predicting the dose outside of the treatment field for a single beam and for multiple beams as used in patient treatment. The phantom was produced in cooperation with the manufacturer of the RANDO® Phantoms (The Phantom Laboratory, Greenwich, NY). It has adjustable body thickness to enhance the verification by more closely simulating the variation in actual patient body size. Since the intra-phantom scatter is an important contributor to the peripheral dose (*18*), the thickness of the patient was recognized to be of importance and worth investigating. Our

custom phantom consists of tissue equivalent material, sliced in the coronal direction, which provides the option of adding or removing slices to create phantoms of different thicknesses while maintaining the anthropomorphic shape (Figure 2). A more detailed description of the new phantom can be found elsewhere (*24*).

In initial investigations, the ability of the PEREGRINE Monte Carlo system to correctly simulate dose outside of the field of a single beam was determined. Results of TLD measurements in the anthropomorphic phantom were compared to Monte Carlo simulations, which were based on CT images of the phantom with the bolus as described above. The TLDs were positioned on the anterior side of the phantom at variable distances from the field edge under the bolus material (2, 8, 10, 12 cm from central beam axis (CAX)). The beam was applied from the posterior side of the phantom, putting the dose points on the beam exit side. Measurements were performed for four different phantom thicknesses (17.9 cm, 25.4 cm, 28.1 cm, 30.7 cm). An open beam (field size 10 x 10 cm2, MLC parked) and an MLC shaped beam were investigated.

Next, multiple beams conditions were verified using the anthropomorphic phantom. Five isocentric fields (gantry angles: 70, 120, 240, 290, and 360 degrees, Varian convention) were directed at the phantom with the isocenter positioned about mid-phantom. The fields were realistically shaped using the MLC. The MLC leafs under the Y jaws were closed and abutted on the side (similar to Figure 1c). Measurements were again performed for four different phantom thicknesses using TLDs placed at 2, 8, 10, and 12 cm from CAX and compared to Monte Carlo simulations based on CT images of the phantoms. All TLD measurements were repeated three times within a measurement series, and two to three measurement series were done for every phantom thickness -

beam setup combination. Therefore at least six independent TLD measurements were performed per data point.

6. Patient Studies

Patients consented for the IRB (Institutional Review Board) approved study received an extra CT scan with bolus covering the anterior side of the treatment region and extending in the superior direction. Based on this CT scan, a treatment plan was created using a clinical 510K-cleared treatment planning system similar to the patient's regular plan and approved by the treating physician. The plan was then submitted for Monte Carlo simulation. Following the simulation, the positions of the dose points of interest on the skin were identified. Based on the phantom measurements we multiplied the doses outside the beam by a factor of 1.15 for the patient simulations (see results section). The patient volunteers had either one or three biopsies at 1 cGy and one or none at 10 cGy, depending on their group within the research protocol. The sites for biopsy were located and marked on the first day of treatment while the patient was in treatment position on the linac couch. A TLD was placed exactly on the position of each biopsy site and another one immediately adjacent to it. TLDs were removed after treatment for readout. As detailed elsewhere (*2*) biopsies were obtained after the first IR fraction.

Sixteen patients have been irradiated. Each patient had two or three irradiated biopsy locations (in addition to a pre-irradiation biopsy). A total of 42 measurement points were taken.

RESULTS

Figure 3 shows the agreement of the phantom measurement for a single open beam (10 x 10 cm^2, MLC parked) with the corresponding Monte Carlo simulations. The difference

of Monte Carlo versus measurement is plotted as a function of distance of measurement point from the CAX for four phantom thicknesses. Three of the thicknesses (25.4 cm, 28.1 cm, 30.7 cm) represent the range of anterior-posterior thicknesses of realistic prostate cancer patients. The thinnest version of the phantom (17.9 cm thickness, left most drawing in Figure 2) is not clinically relevant and was examined only in order to gain insight into simulation-measurement deviation trends.

For the measurement points outside the field, as shown in Figure 3, Monte Carlo simulations are 5% less than measurements for off axis locations greater than 8 cm. At 8 cm off axis the agreement is within 3 %, and at a control point inside the field (2 cm of CAX, not shown here) the agreement is better than 2%, which is well within the error of TLD measurement.

With a single MLC shaped beam (as in Figure 1c) the deviation of off-axis simulations and measurements was greater as shown in Figure 4a. When examined as a function of phantom thickness, simulations increasingly underestimate the dose with decreasing phantom thickness (Figure 4b).

Figure 5 shows agreement for five-beam cases, where four oblique beams are added to the PA beam. All beams are MLC-shaped for a standard prostate cancer treatment in the way illustrated in Figure 1c. These additional beams increase the deviation of the Monte Carlo simulations from the measurements to approximately 8-22% with a trend of increasing deviation with distance from the CAX. Figure 5a illustrates the dependence of the deviation on the distance of the measurement point from the CAX. Figure 5b shows the relationship between the phantom thickness and the percentage deviation of the Monte Carlo simulation and the measurements. For five-field cases significant thickness dependence was not observed.

While the deviations described above are of scientific interest from a physics research perspective, they did not hinder the progress of the biology component of the project. We found that within the range of clinical patient thicknesses (phantom thicknesses 25.4-30.7 cm,) at the doses required for the biologic investigations (1 cGy and 10 cGy), a single, thickness-independent correction factor of 1.18 could be applied to the results of Monte Carlo simulations to yield a reliable prediction for the biopsy location in a clinical setting.

Figure 6 shows the dose measured at the predicted 1 cGy biopsy points in 16 (consecutive) patients. The average dose measured with TLD on the biopsy location predicted by the corrected Monte Carlo algorithm to receive 1 cGy was 0.985 cGy (Standard deviation: 0.110 cGy). The additional TLD adjacent to the biopsy location measured on average 1.00 cGy (Standard deviation: 0.105 cGy). The data for all 1 cGy points is displayed in figure 6 showing an overall very good agreement.

The 10 cGy points presented a greater challenge because the points were located within a high dose gradient region. For the six patients that underwent biopsies for 10 cGy, the average measured dose at the location of the biopsy was 5.90 cGy (Standard deviation: 1.01 cGy) and adjacent to the location 5.84 cGy (Standard deviation: 1.80 cGy) (see Figure 7). This deviation is equivalent to an approximately 6 mm shift in the biopsy position from the field edge as illustrated for a typical case in Figure 8.

DISCUSSION

Translational human data is an essential key in the investigation of the effects of LDIR on humans. In patients receiving therapeutic radiation there exists a wide range of dose points, from very low doses through to the maximum dose given in a treatment fraction. This range can be used for the *in vivo* investigation of the effects of low doses of ionizing radiation on humans if the biopsy site is accessible in the clinic and if dose prediction at the potential biopsy site can be performed accurately. We have reported details of our investigations of the practicality of predicting the location of skin surface dose at potential biopsy sites outside the treatment field that receive 1 cGy and 10 cGy for prostate radiotherapy patients.

This methodology was sufficiently accurate to support the clinical/biological investigations. It also has also revealed interesting discrepancies between Monte Carlo simulations and measurements. The phantom measurements showed that outside the field, dose calculation with Monte Carlo simulations are systematically lower than measurements using TLDs. This is true even for the simplest case of a single beam with parked MLC (measurements on the beam exit side of the phantom). The effect is noticeable starting between 8 and 10 cm from CAX (10x10 cm^2 field). The deviation increases for an MLC shaped beam and even more for a five beam treatment using MLC. The deviation is larger as distances increase from the CAX under all examined cases. Influence of the phantom thickness was observed for the single beam MLC shaped experiments (Fig 4b). For thicker phantoms the deviation is smaller, indicating that the discrepancy stems at least in part from simplifications in the simulation of the accelerator head; the longer path of the radiation to the detector through a thicker phantom reduces the impact. This is consistent with the Monte Carlo simulations failing to accurately

model dose components originating outside the main beam line in the accelerator head. With the addition of the MLCs to the beam shaping and simulations, problems may arise from the simulation of either the MLC transmission properties or scatter off the MLCs into regions outside the field. Thicker phantoms have a larger solid angle subtended at the TLD and therefore a larger fraction of the dose comes from intra-phantom scatter. In turn, this leads to a smaller dependence on accuracy of simulation of the beam line than in the very thin phantom case, consistent with our results.

The addition of oblique beams, as used in the five beam cases, further increases the difference between simulation and measurement. This can be best explained by increased accelerator head scatter reaching the measurement points of interest with less intra-phantom attenuation, as compared to the AP beam.

Within the parameters of a clinical prostate cancer treatment, a single, thickness-independent correction factor can be used to identify biopsy locations outside the beam. Locations receiving 1 cGy in one fraction of regular 5-beam prostate cancer therapy (2 Gy at 95% isodose line) could be identified with high reliability (average dose: 0.985 cGy, standard deviation: 0.110 cGy, which represents 0.05% of the prescribed dose). Under the same conditions, 10 cGy points are harder to pre-specify since they are located in the high dose gradient of the field edge. This is illustrated in figure 8, which shows the dose along the midline of a patient under the bolus material for a single protate treatment fraction (2 Gy at 95% isodose line). The 1 cGy point (filled diamond) is located in a low gradient area well outside the field. The 10 cGy point (filled square) is at the edge of the field in a very steep dose gradient. Considering the circumstances of a

real-world treatment, including the fact that the patient is breathing, small movements of the biopsy site throughout the treatment cannot be avoided. For the 10 cGy point, however, such small movements have drastic consequences. As shown in figure 8, moving the point on the skin by just 6 mm causes the dose received to drop to the measured average of 5.9 cGy (open square). Therefore large percentage deviations correspond to only small shifts of the biopsy point with respect to the field edge (about 6 mm), which are well within the range of expected movement. Thus, the Monte Carlo CT based method of dose prediction presented here is in itself not sufficient to operate in such dose gradients. A modification of the protocol to address this challenge is under development. However, for the 1 cGy point the present method delivers accuracy with high reliability and has allowed important biologic studies to proceed.

ACKNOWLEDGMENTS

This work was performed under the auspices of the U.S. Department of Energy by University of California Lawrence Livermore National Laboratory under contract No. W-7405-Eng-48 and supported in part by the Office of Science (BER), U.S. Department of Energy, Grant No. DE-FG03-01ER63237.

This work has been presented in part at the ASTRO 44th Annual meeting, New Orleans 2002, the World Congress of Medical Physics and Biomedical Engineering, Sydney 2003 and the 12th International Conference on Radiation Research in Brisbane 2003.

The authors would like to thank Cynthia A. Fix of LLNL for the reliable support in preparing and reading out the Thermoluminescence dosimeters (TLD).

REFERENCES

1. S. A. Amundson, K. T. Do and A. J. Fornace, Jr., Induction of stress genes by low doses of gamma rays. *Radiat Res* **152,** 225-231 (1999).
2. Z. Goldberg, C. W. Schwietert, R. L. Stern, M. Arnold, C. L. Hartmann Siantar, R. Cary, J. Lehmann and B. E. Lehnert, Exposure to Low Dose (1-10 cGy) Ionizing Radiation: Assessment of Effects in Humans and Relevance to Cancer. *Int. J. Radiat. Oncol. Biol. Phys.* **54,** 53 (2002).
3. Central axis depth dose data for use in radiotherapy. *Br J Radiol Suppl* **25,** 1-188 (1996).
4. B. A. Fraass and J. Van De Geijn, Peripheral dose from megavolt beams. *Med Phys* **10,** 809-818 (1983).
5. P. H. Van Der Giessen, Calculation and measurement of the dose at points outside the primary beam for photon energies of 6, 10, and 23 MV. *Int J Radiat Oncol Biol Phys* **30,** 1239-1246 (1994).
6. M. Stovall, C. R. Blackwell, J. Cundiff, D. H. Novack, J. R. Palta, L. K. Wagner, E. W. Webster and R. J. Shalek, Erratum: 'Fetal dose from radiotherapy with photon beams: report of AAPM Radiation Therapy Committee Task Group No. 36'[Med. Phys. **22**, 63-82 (1995)]. *Med Phys* **22,** 1353-1354 (1995).
7. M. Stovall, C. R. Blackwell, J. Cundiff, D. H. Novack, J. R. Palta, L. K. Wagner, E. W. Webster and R. J. Shalek, Fetal dose from radiotherapy with photon beams: report of AAPM Radiation Therapy Committee Task Group No. 36. *Med Phys* **22,** 63-82 (1995).

8. R. L. Stern, Peripheral dose from a linear accelerator equipped with multileaf collimation. *Med Phys* **26,** 559-563 (1999).

9. S. Sherazi and K. R. Kase, Measurements of dose from secondary radiation outside a treatment field: effects of wedges and blocks. *Int J Radiat Oncol Biol Phys* **11,** 2171-2176 (1985).

10. S. C. Sharma, J. F. Williamson, F. M. Khan and C. K. Lee, Measurement and calculation of ovary and fetus dose in extended field radiotherapy for 10 MV x rays. *Int J Radiat Oncol Biol Phys* **7,** 843-846 (1981).

11. A. Sanchez-Reyes, M. Ginjaume, H. Chakkor, A. Melero, F. Pons and X. Ortega, Estimation of peripheral dose from two linacs: Mevatron MX6700 and Mevatron KDS. *Med Dosim* **19,** 83-87 (1994).

12. J. Novotny and M. S. Tarakanath, Radiation protection of the patient during radiotherapy. *Strahlentherapie* **152,** 191-198 (1976).

13. A. Niroomand-Rad and R. Cumberlin, Measured dose to ovaries and testes from Hodgkin's fields and determination of genetically significant dose. *Int J Radiat Oncol Biol Phys* **25,** 745-751 (1993).

14. S. Mutic and D. A. Low, Whole-body dose from tomotherapy delivery. *Int J Radiat Oncol Biol Phys* **42,** 229-232 (1998).

15. S. Mutic and E. E. Klein, A reduction in the AAPM TG-36 reported peripheral dose distributions with tertiary multileaf collimation. American Association of Physicists in Medicine Task Group 36. *Int J Radiat Oncol Biol Phys* **44,** 947-953 (1999).

16. S. Mutic, J. Esthappan and E. E. Klein, Peripheral dose distributions for a linear accelerator equipped with a secondary multileaf collimator and universal wedge. *J Appl Clin Med Phys* **3,** 302-309 (2002).

17. B. J. Mcparland and H. I. Fair, A method of calculating peripheral dose distributions of photon beams below 10 MV. *Med Phys* **19,** 283-293 (1992).

18. K. R. Kase, G. K. Svensson, A. B. Wolbarst and M. A. Marks, Measurements of dose from secondary radiation outside a treatment field. *Int J Radiat Oncol Biol Phys* **9,** 1177-1183 (1983).

19. D. Greene, P. G. Karup, C. Sims and R. J. Taylor, Dose levels outside radiotherapy beams. *Br J Radiol* **58,** 453-456 (1985).

20. D. Greene, G. L. Chu and D. W. Thomas, Dose levels outside radiotherapy beams. *Br J Radiol* **56,** 543-550 (1983).

21. P. Francois, C. Beurtheret and A. Dutreix, Calculation of the dose delivered to organs outside the radiation beams. *Med Phys* **15,** 879-883 (1988).

22. S. Bieri, M. Russo, M. Rouzaud and J. M. Kurtz, Influence of modifications in breast irradiation technique on dose outside the treatment volume. *Int J Radiat Oncol Biol Phys* **38,** 117-125 (1997).

23. C. L. Hartmann Siantar, R. S. Walling, T. P. Daly, B. Faddegon, N. Albright, P. Bergstrom, A. F. Bielajew, C. Chuang, D. Garrett, R. K. House, *et al.*, Description and dosimetric verification of the PEREGRINE Monte Carlo dose calculation system for photon beams incident on a water phantom. *Med Phys* **28,** 1322-1337 (2001).

24. J. Lehmann, R. Stern, J. Levy, T. P. Daly, C. L. Hartmann Siantar and Z. Goldberg, Radiation phantom with humanoid shape and adjustable thickness (RPHAT). *Phys Med Biol* **49,** N125-N129 (2004).

FIGURE LEGENDS

FIG. 1. Schematic of an MLC shaped field with (a) the MLC leaves closed under the Y2 jaw in standard 0,0 position, (b) the MLC leaves open under the Y2 jaw and (c) the MLC leaves set to –7,7 under the Y2 jaw to avoid abutting the leaves directly over the points of interest (filled circles).

FIG. 2. Custom anthropomorphic phantom with variable thickness. Shown are the thinnest (left) and the thickest (right) version and one in between configuration. The phantom is described in more detail in reference (*24*).

FIG. 3. Comparison of the phantom measurements with the corresponding Monte Carlo simulations for a single open beam (isocentric setup, 10 x 10 cm^2, MLC parked) for four phantom configurations: very thin (17.9 cm thick), thin (25.4 cm), medium (28.1 cm) and thick (30.7 cm). The y-axis shows the %difference between simulations (PG) and TLD measurements (TLD): (PG-TLD)/TLD. The x-axis represents the distance of measurement point from the CAX. The error bars shown in this and in all subsequent diagrams represent one standard deviation.

FIG. 4. Comparison of the phantom measurements with the corresponding Monte Carlo simulations for a single MLC shaped beam (isocentric setup, 10 x 10 cm^2, MLC leaves under the jaws closed on the side as in Figure 1c) for four phantom configurations: very thin (17.9 cm thick), thin (25.4 cm), medium (28.1 cm) and thick (30.7 cm). The y-axis shows the %difference between simulations (PG) and TLD measurements (TLD): (PG-TLD)/TLD. The %difference is plotted as a function of distance of measurement point from the CAX for the four phantom thicknesses (a) and as a function of phantom thicknesses for three distances of the measurement point from the CAX (b).

FIG. 5. Comparison of the phantom measurements with the corresponding Monte Carlo simulations for a realistic 5 beam prostate treatment (isocentric setup, 10 x 10 cm^2, MLC leaves under the jaws closed on the side as in Figure 1c) for four phantom configurations: very thin (17.9 cm thick), thin (25.4 cm), medium (28.1 cm) and thick (30.7 cm). The y-axis shows the %difference between simulations (PG) and TLD measurements (TLD): (PG-TLD)/TLD. The %difference is plotted as a function of distance of measurement point from the CAX for the four phantom thicknesses (a) and as a function of phantom thicknesses for three distances of the measurement point from the CAX (b).

FIG. 6. TLD measurements at locations on patients that were pre-selected to receive 1 cGy (filled diamonds) and adjacent to the locations (open squares). Patients 1-6 had each one 1 cGy biopsy location, patients 7-16 had each three locations. Average dose on the location was 0.985 cGy (Standard deviation: 0.110 cGy) and adjacent to the location 1.00 cGy (Standard deviation: 0.105 cGy).

FIG. 7. TLD measurements at locations on patients that were pre-selected to receive 10 cGy (filled diamonds) and adjacent to the locations (open squares). Average dose on the location was 5.90 cGy (Standard deviation: 1.01 cGy) and adjacent to the location 5.84 cGy (Standard deviation: 1.80 cGy).

FIG. 8. Dose along the midline of a typical patient under the bolus material from a single protate treatment (2 Gy at 95% isodose line). The 1 cGy point (diamond) is located in a low gradient area well outside the field. The 10 cGy point (filled square) is at the edge of the field in a very steep dose gradient. The average measurement for the 10 cGy points (figure 7) was 5.9 cGy (open square), which is for this typical case about 6 mm away from the location with the desired 10 cGy.

FOOTNOTES

[1] MLC leaf positions are described according to the Varian convention: The first number corresponds to the position of the leaf of the leaf bank A (under X1 jaw) and describes the position of this leaf as the distance of its tip from the field midline in the projection to the isocenter plane in units of centimeter. The second number describes the leaf of the leaf bank B (under X2 jaw) accordingly. Negative numbers indicate overtravel, that is a leaf crossing the midline.

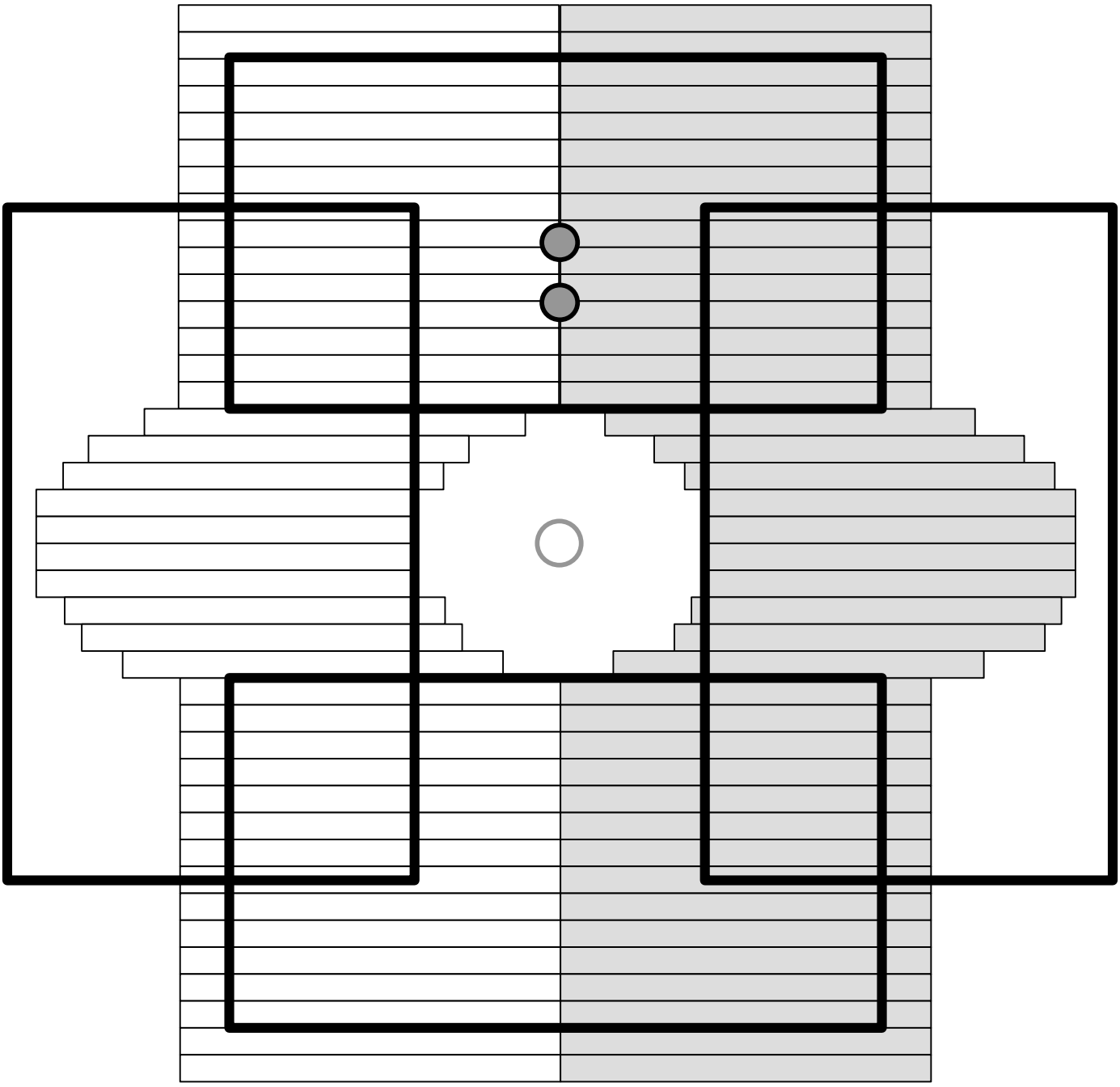

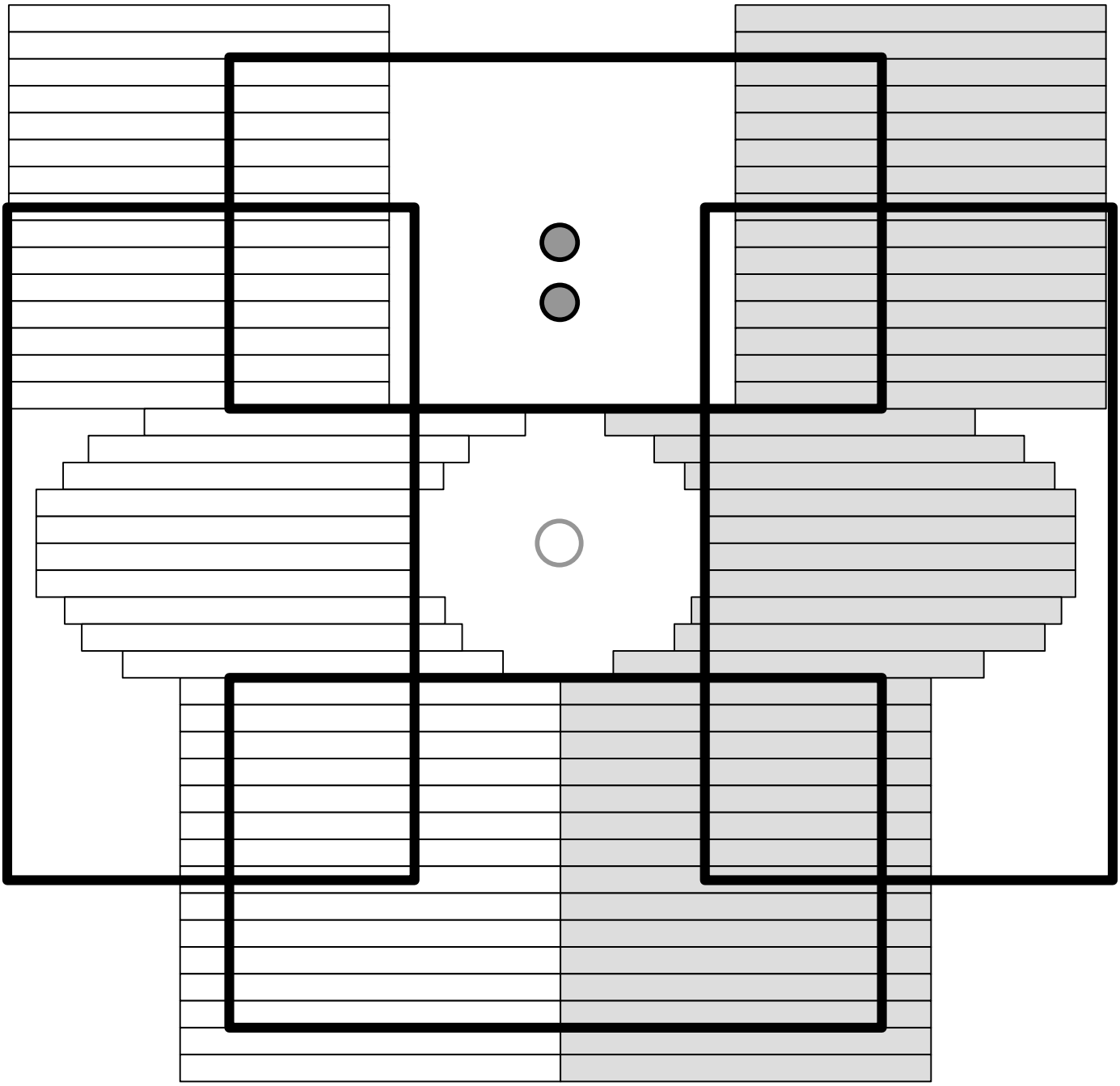

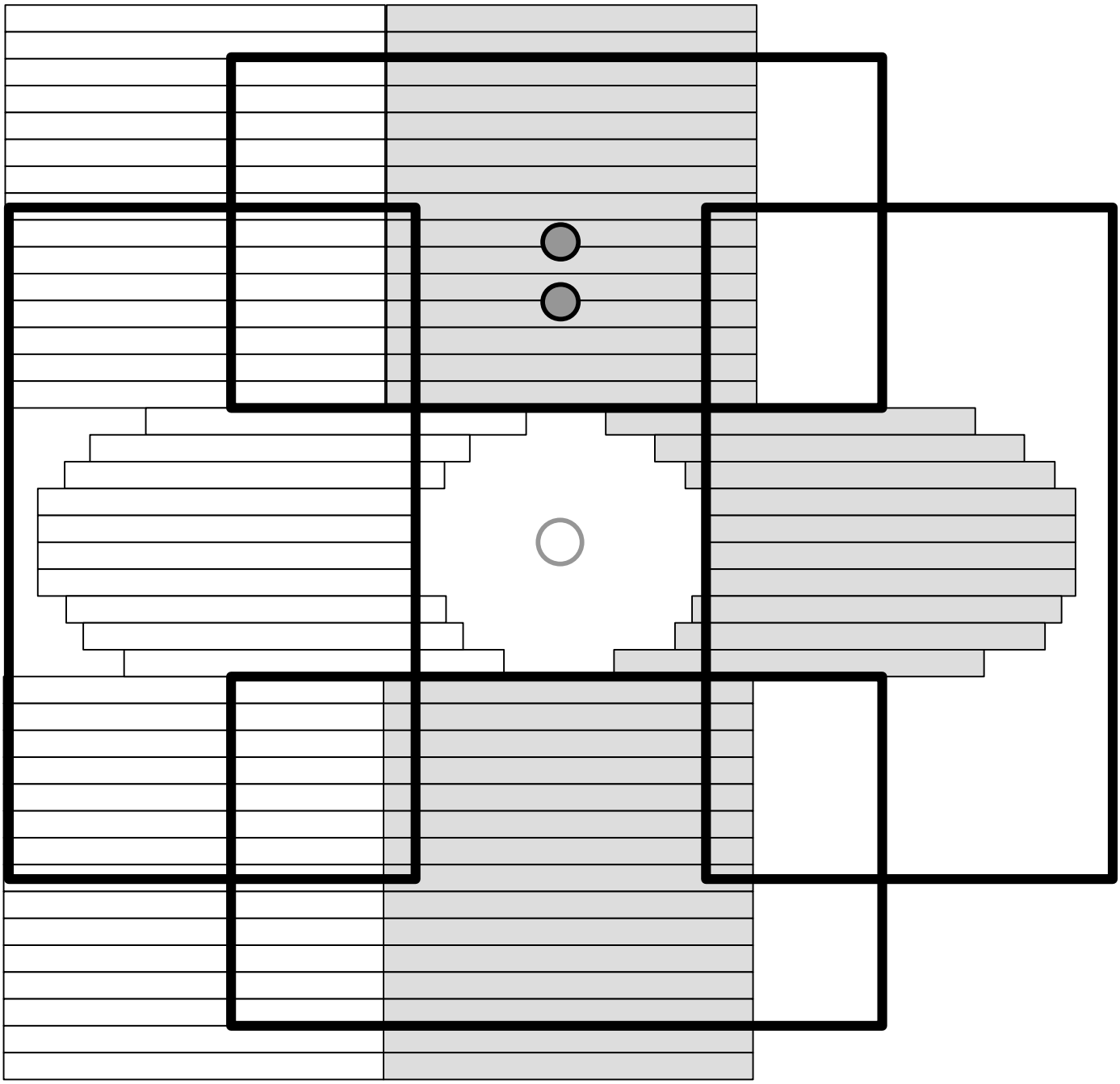

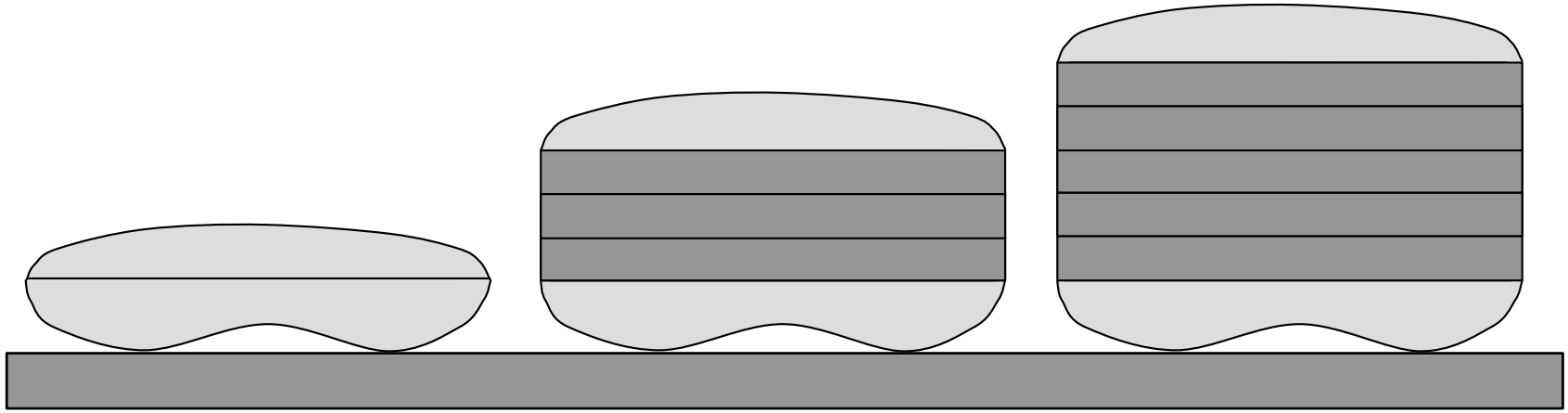

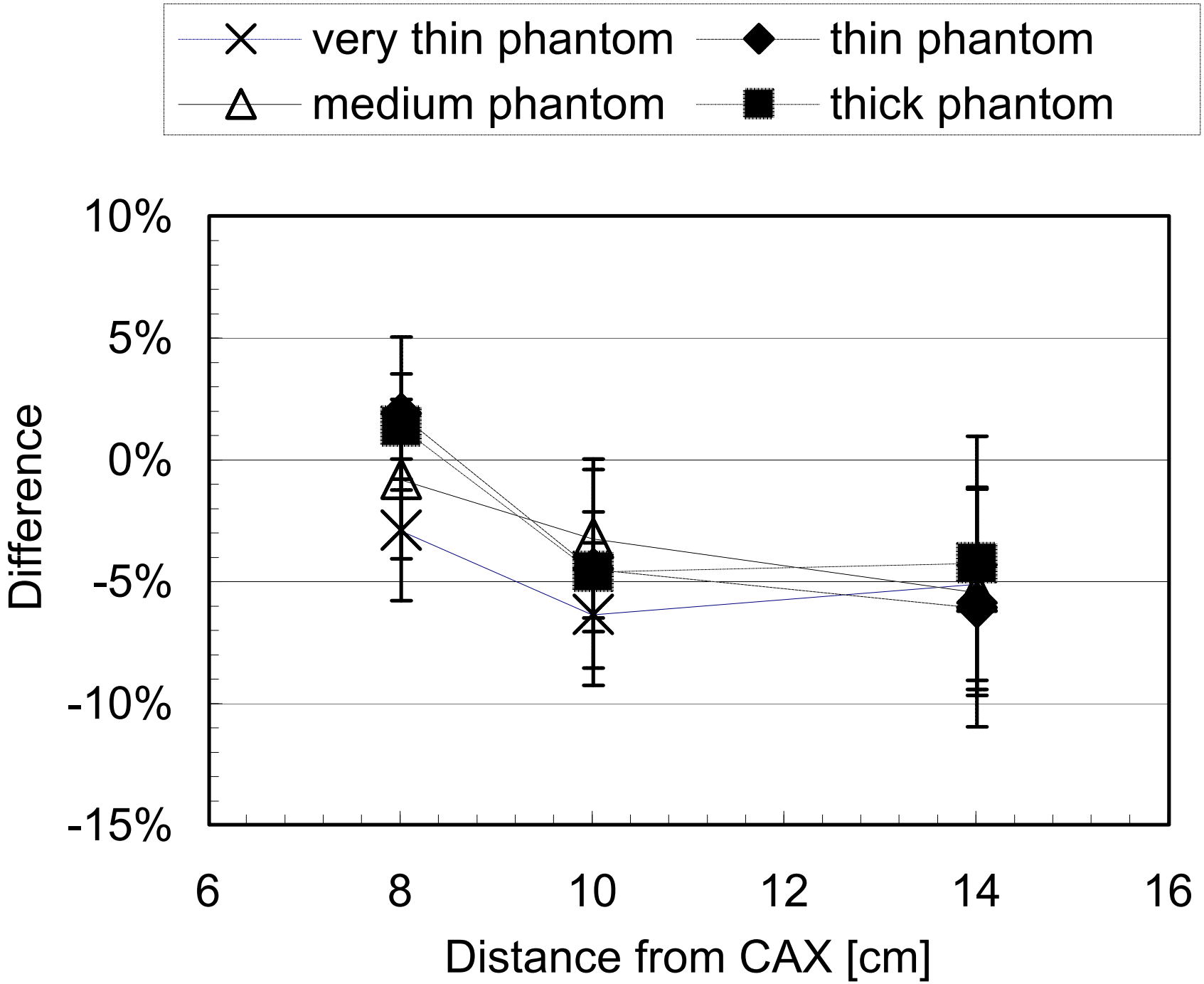
very thin phantom
thin phantom
medium phantom
thick phantom
10%
5%
0%
-5%
-10%
-15%
Difference
6
8
10
12
14
16
Distance from CAX [cm]

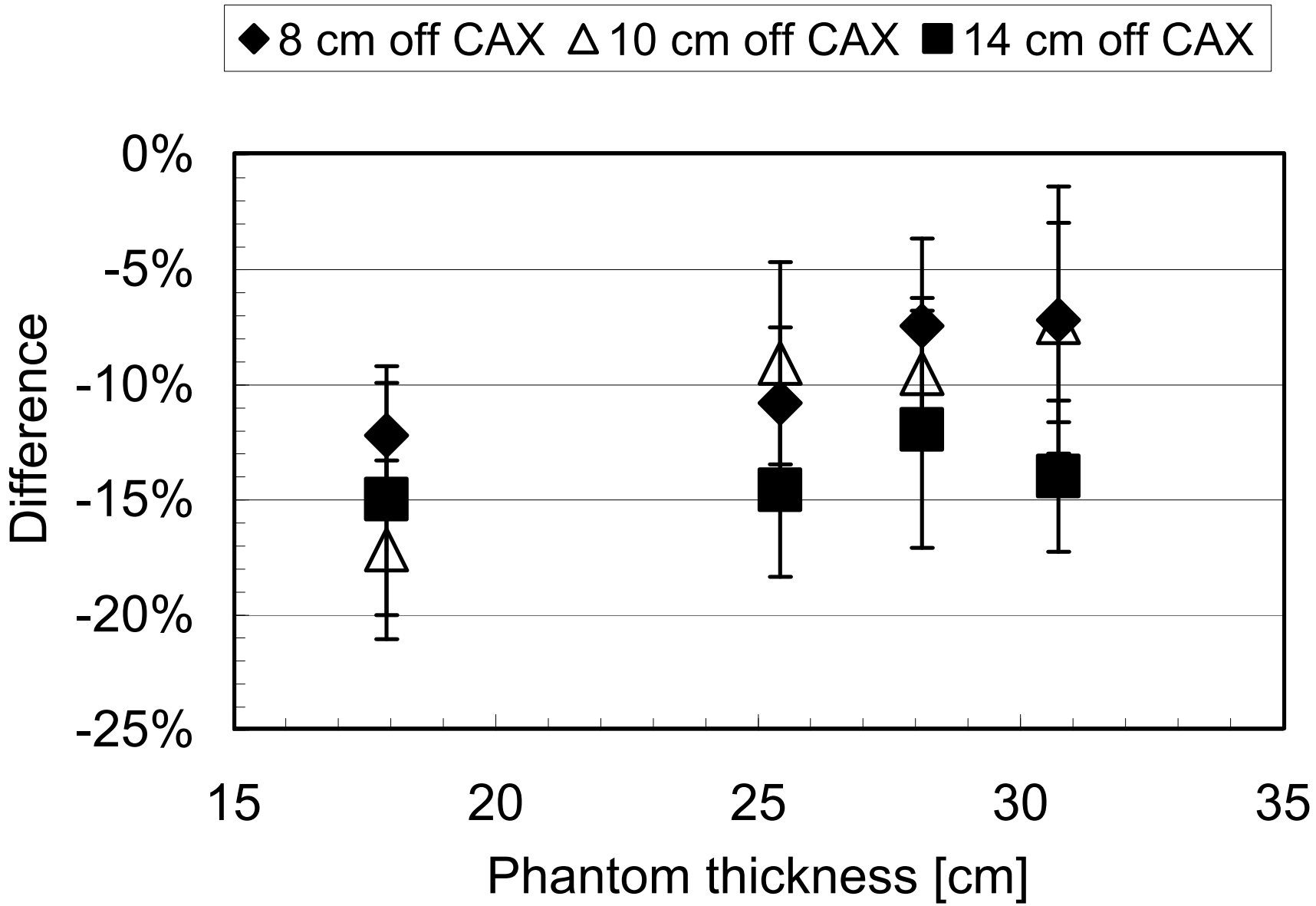
8 cm off CAX
10 cm off CAX
14 cm off CAX
0%
-5%
-10%
-15%
-20%
-25%
Difference
15
20
25
30
35
Phantom thickness [cm]

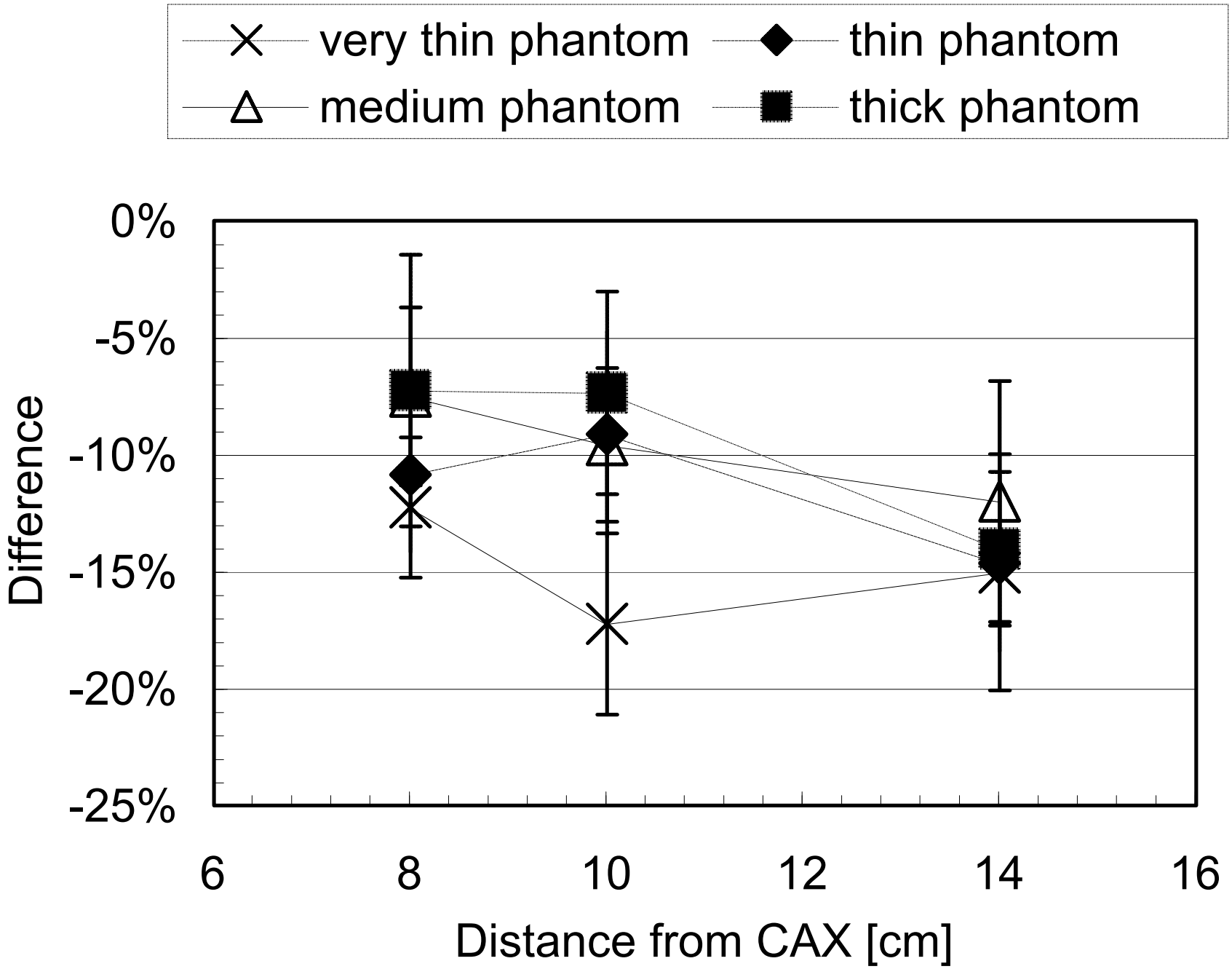
very thin phantom
thin phantom
medium phantom
thick phantom
0%
-5%
-10%
-15%
-20%
-25%
Difference
6
8
10
12
14
16
Distance from CAX [cm]

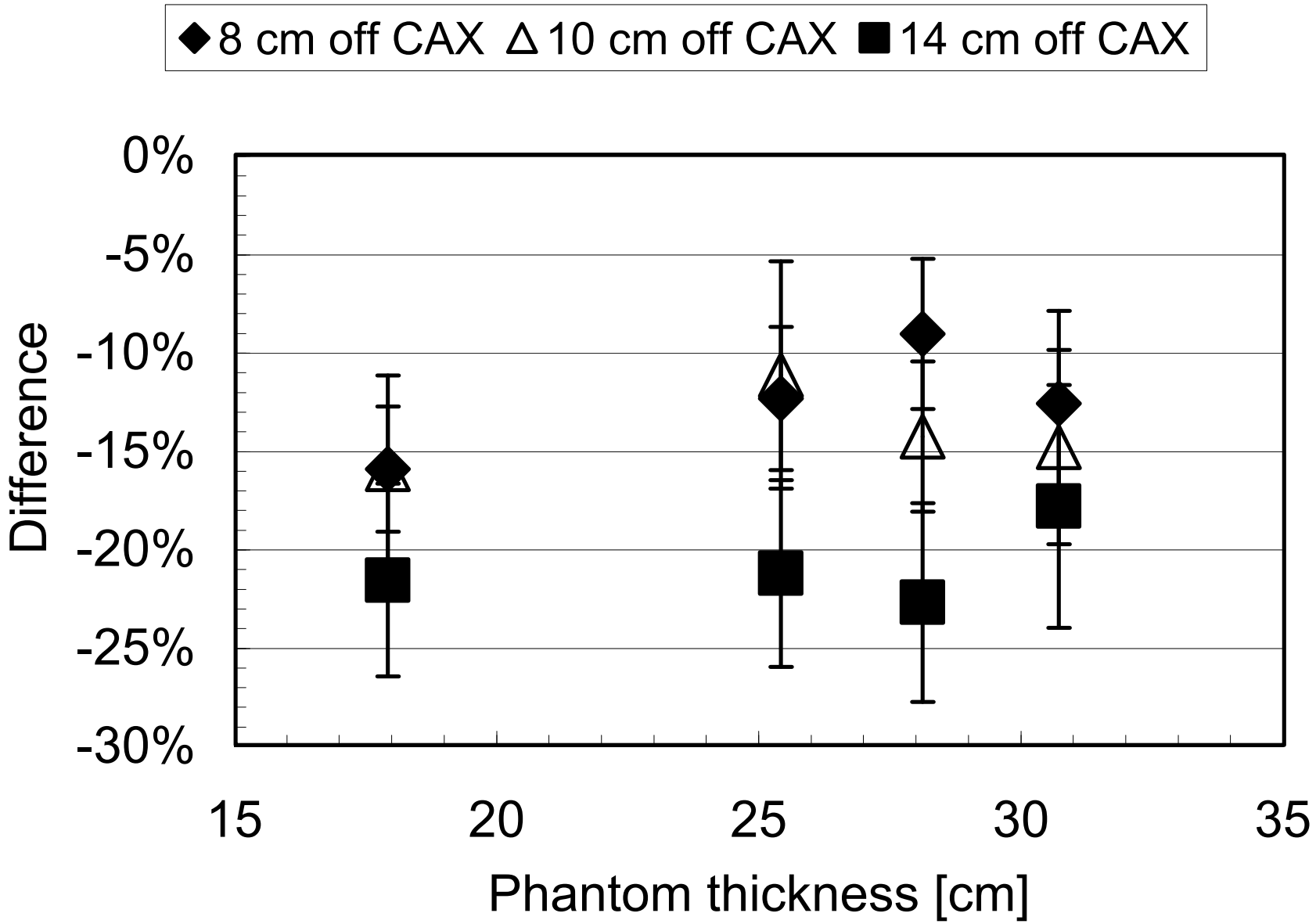
◆8 cm off CAX
Δ10 cm off CAX
■14 cm off CAX
0%
-5%
-10%
-15%
-20%
-25%
-30%
Difference
15
20
25
30
35
Phantom thickness [cm]

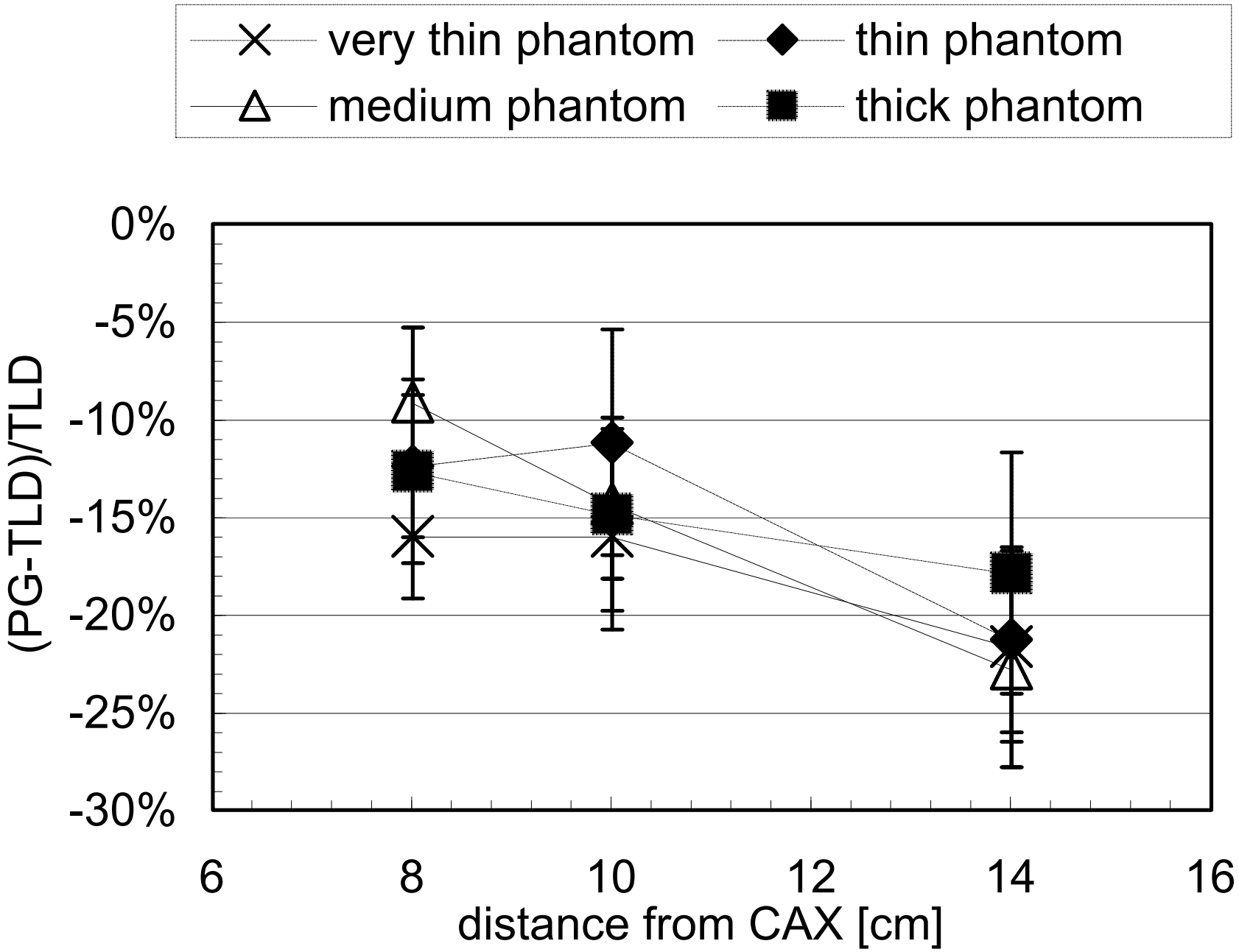
very thin phantom
thin phantom
medium phantom
thick phantom
0%
-5%
-10%
-15%
-20%
-25%
-30%
(PG-TLD)/TLD
6
8
10
12
14
16
distance from CAX [cm]

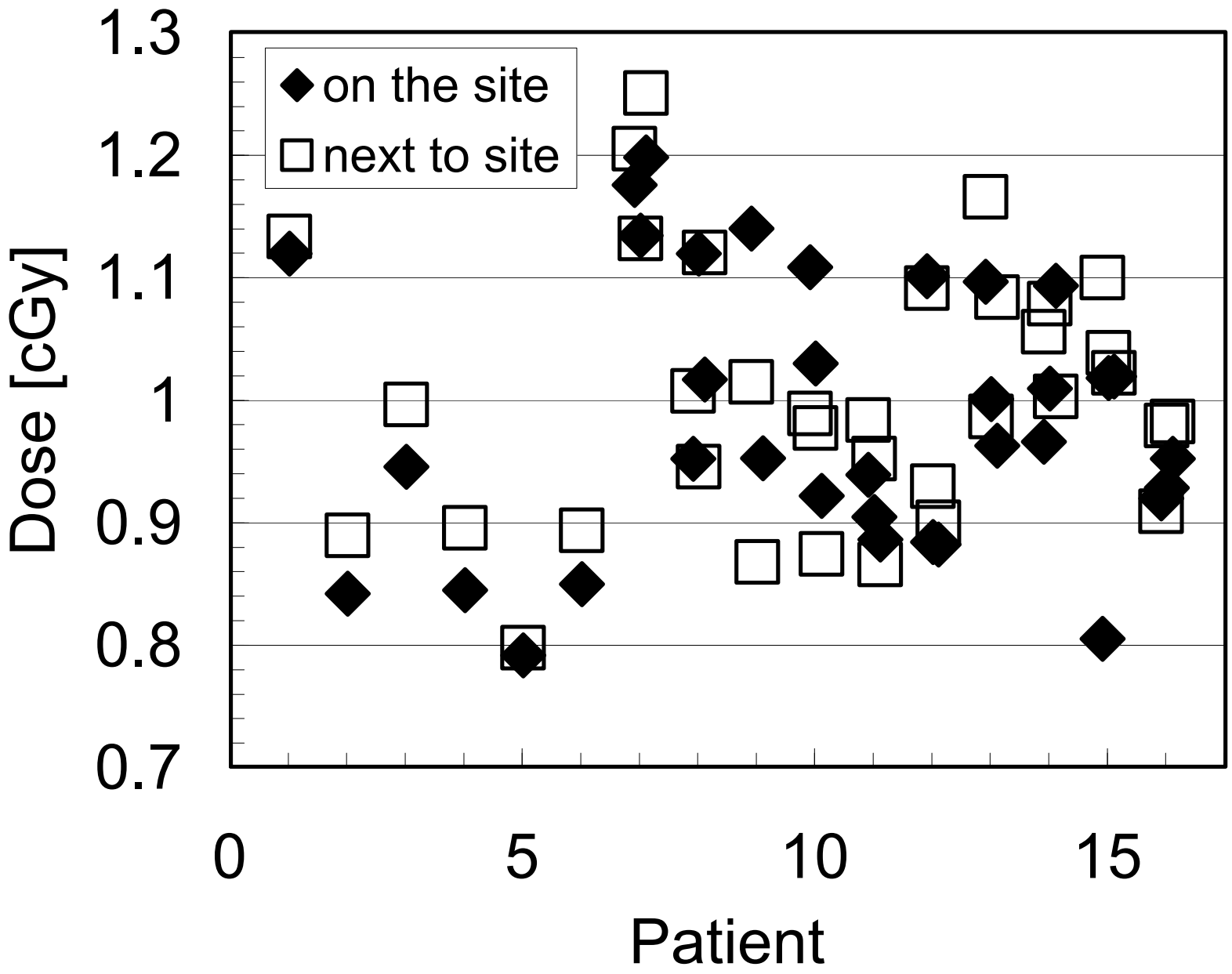
on the site
next to site
Dose [cGy]
1.3
1.2
1.1
1
0.9
0.8
0.7
0
5
10
15
Patient

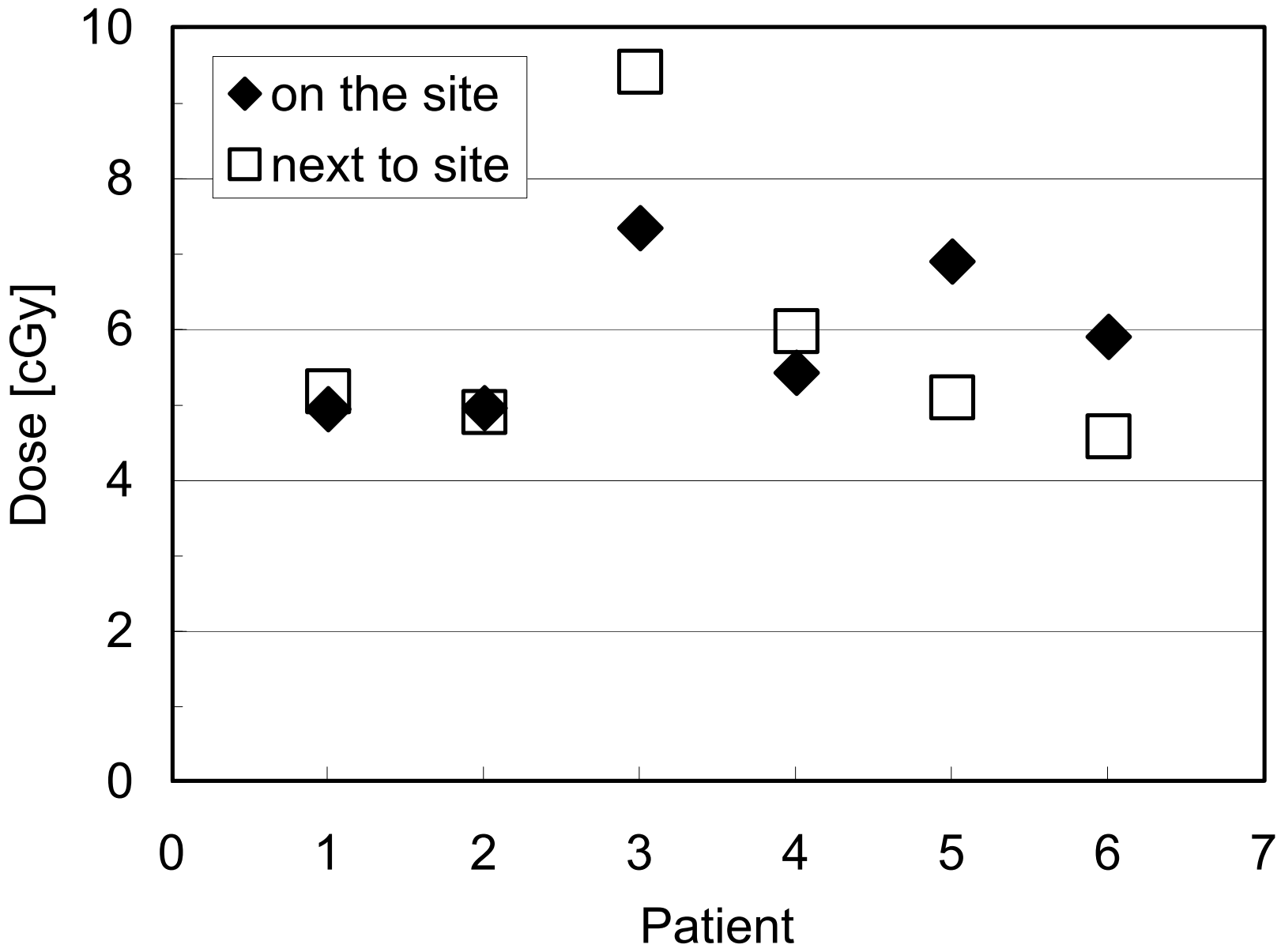
10
8
6
4
2
0
Dose [cGy]
on the site
next to site
0
1
2
3
4
5
6
7
Patient

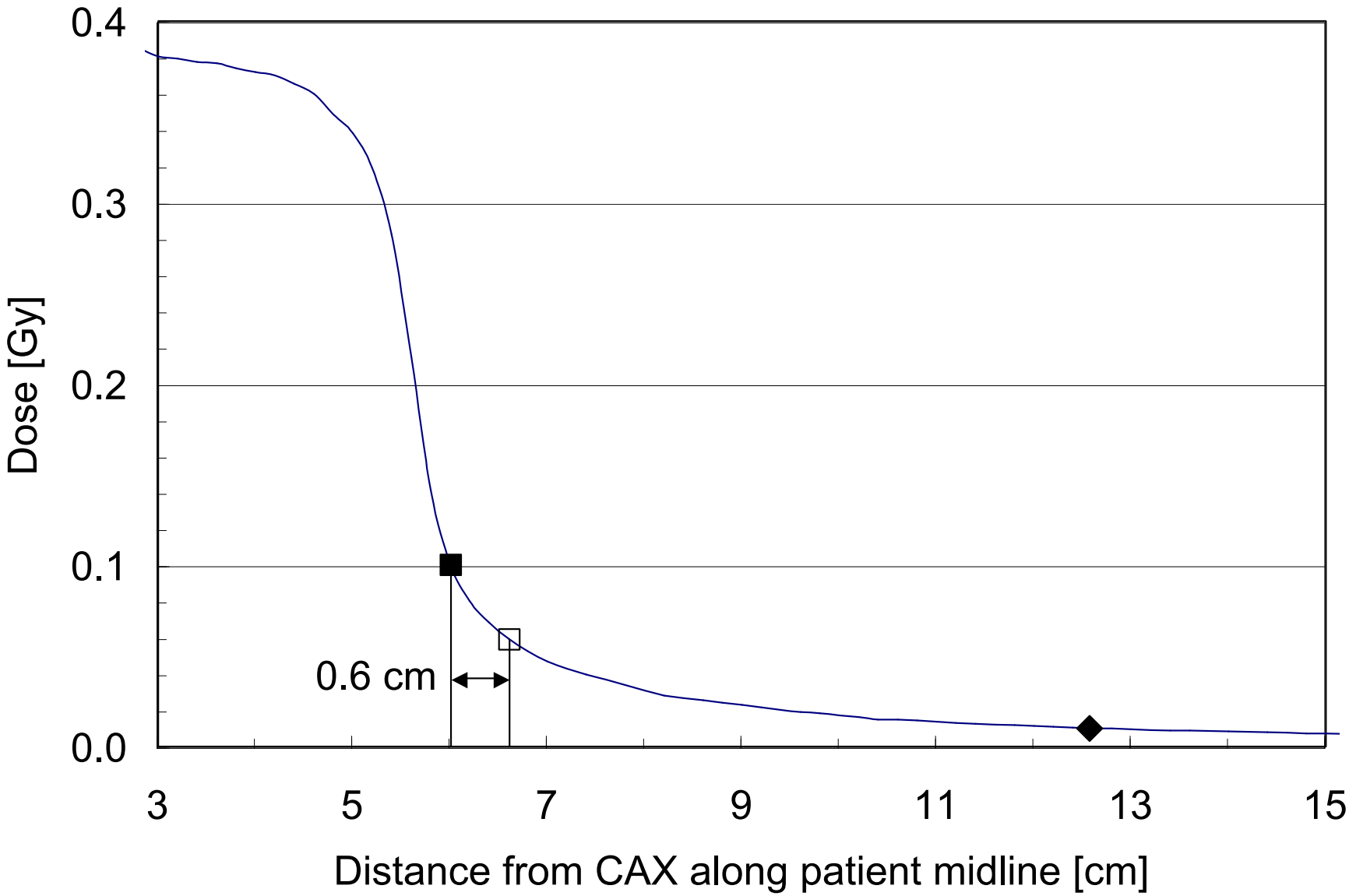
0.4
0.3
0.2
0.1
0.0
Dose [Gy]
0.6 cm
3
5
7
9
11
13
15
Distance from CAX along patient midline [cm]